ISSN 1330-3651 (Print), ISSN 1848-6339 (Online)
Received: 30 June 2025; Accepted: 18 November 2025

https://doi.org/10.17559/TV-20250603002721
Original scientific paper

Dynamics of a Rigid Body During a Slipping Motion on a Vibratory Conveyor

Uroš ILIĆ*, Mihailo LAZAREVIĆ, Emil VEG, Željko DESPOTOVIĆ, Nenad GUBELJAK

Abstract: This paper presents research on the optimisation of a vibratory transport on an assembly line. The study covers a special case of vibratory transport characterised by uninterrupted contact between the transported body and the vibratory trough's surface, and the interaction is modelled using Coulomb's model with stiction. In the first phase of the research, an analysis of external forces acting on the body during relative motion is conducted, and the conditions for non-hopping vibratory regimes are defined. The differential equations of relative motion are derived, and the precise moments at which relative sliding on the vibratory conveyor occurs are analytically determined. The proposed theoretical model of vibratory motion is validated with computer simulations performed in SolidWorks Motion Analysis. The obtained simulation results confirm the analytical predictions and are discussed in detail at the end of the paper.

Keywords: CAD simulation; coulomb friction; relative motion; vibratory conveyor

1 INTRODUCTION

The problem of materials' internal transport is usually performed in some sort of conveyance process. Apart from regular belt conveyors [1] that move material in continuous motion, vibratory conveyors put material into motion via some form of oscillating actuator. That actuator could be mechanical, in form of a camshaft mechanism [2, 3] or electromagnetic [4, 5].

A standard and most cost-effective vibratory conveyor design is one with a horizontal track with inclined direction of the vibrations' source. Vibration angle in a single degree of freedom actuators is defined by placement of the leaf springs that support the vibratory trough. Leaf springs are placed with an angle that goes from 0 to 45° with the optimal value of $\alpha = 20°$ [4, 6].

Regardless of their design, each conveyor transports material in similar fashion, in a hopping or no-hopping motion - depending whether the material leaves the surface of the vibratory trough. Hopping motion produces larger mass flow at the trough's exit, but this motion cannot be represented analytically with sufficient accuracy. Theoretical models do exist, but they are hard to be proven experimentally [7-10]. This especially holds for grain-like structures, where it is not possible to derive an analytical solution. In this case methods from statistical mechanics or numerical estimations by a computer are used to estimate the conveyance process [11].

On the other side, a non-hopping motion is sometimes needed to provide steady and controlled mass flow or when transported material is delicate, sensitive or needs to be transported in predetermined orientation [12, 13]. This form of motion is characterized with constant contact between the conveyed material and the vibratory surface. Unlike granular materials, the conveyed object maintains its structural integrity and moves as a single rigid entity. It starts to slide in the backstroke of the actuator, when the inertial forces surpass the intensity of the friction forces. This is achieved either by manipulating the intensity of the vertical acceleration [10, 12-14] or even by modification of horizontal vibration's parameters of the trough [15, 16].

The main problem of any analytical solution to the vibratory conveyance is trying to find an optimal mathematical model of the dissipative friction force. Numerous theories explain the concept of friction between two bodies. The simplest one is Coulomb's dry friction model [17-19] that uses a single friction coefficient μ. An enhancement of this model is Coulomb's friction that supports so-called stiction phenomena, the fact that the contact force rapidly drops after the relative slipping starts [16]. Some contemporary friction models try to overcome this discontinuity issue by employing different non-linear functions. For example the Benson model presented in [21] employs smooth transition from peak values of friction force to its dynamic values when the motion starts. There are others, more complicated models that are centred around tribology and contact mechanics theory that can be found in the literature [16, 19-21].

This research focuses on steady, non-hopping vibratory transport of an object with a complex shape, where the term complex indicates that the transported object has a small number of symmetries. Therefore, it must reach a specific orientation at the end of the transport. This is typically required in automated or robotized assembly lines, where a robot needs to pick up a machine element (e.g., gears, screws, nuts, bushings) in the exact orientation each time in order to properly insert it into the given assembly.

2 DYNAMIC ANALYSIS OF THE RELATIVE MOTION

The problem of analysing the motion of the object with a complex shape during the non-hopping vibratory transport will be approached through the study of the dynamics of relative motion of a rigid body inside a non-inertial reference frame, as illustrated in the Fig. 1. For the purposes of this research, it is assumed that the massive base of the vibratory conveyor is stationary during the vibratory process.

The absolute coordinate system *Oxy* is rigidly attached to the centre of mass of the stationary base, while the non-inertial reference frame $O_1\xi\eta$ is rigidly attached to the centre of mass of the vibratory trough. The rigid body of mass *m*, moves in the non-inertial reference frame and the relative position vector of its centre of mass is given by $\vec{\rho}$. The position vector in the absolute coordinate system is therefore given with $\vec{r} = \vec{r}_0 + \vec{\rho}$.

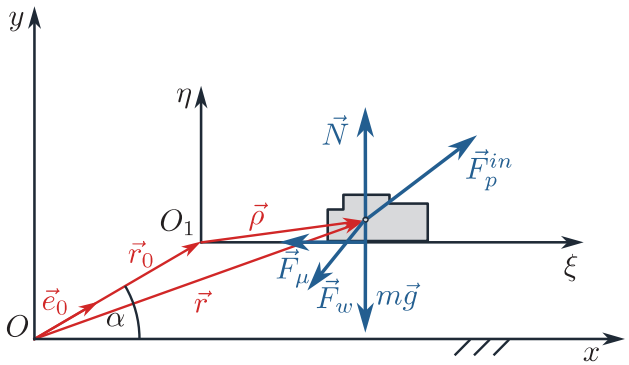

Figure 1 Position of the rigid body inside absolute and relative coordinate systems

The unit vector $\vec{e}_0$ forms an angle α with respect to the horizontal axis and represents a technical characteristic of the conveyor itself. During the operation of the vibratory conveyor, the change of the vector $\vec{r}_0$ defines the change in distance between the centre of mass of the vibratory trough and the centre of mass of the stationary base. In a general case, a vibratory actuator is given by:

$$\vec{r}_0 = |\vec{r}_0(t)| \cdot \vec{e}_0(t) = A\sin\omega t \cdot \vec{e}_0(t) \tag{1}$$

where A represents the amplitude of the actuator's motion, $\omega = 2\pi \cdot f$ is the angular frequency of oscillatory motion and $\vec{e}_0(t)$ is the unit vector that defines the relative direction between the trough and the base. For small deflections around the resting point, the relative motion of the vibratory trough can be assumed as rectilinear and planar [4, 7, 22], hence $\vec{e}_0 = \text{const.} = \begin{pmatrix}\cos\alpha & \sin\alpha & 0\end{pmatrix}^T$. Also, with an appropriate control system one can assume that ω and A of the actuator's vibrations remain constant during the operation of the vibratory conveyor.

Following on, body's relative acceleration $\vec{a}_r$ is equivalent to its acceleration in the non-inertial reference frame and it is equal to $\vec{a}_r = \ddot{\vec{\rho}}(t) = \begin{pmatrix}\ddot{\xi}(t) & \ddot{\eta}(t) & 0\end{pmatrix}^T$.

2.1 Analysis of the External Forces That Act on the System

A free body diagram from Fig. 1 can be expressed mathematically with a vector equation of motion:

$$m\vec{a}_r = m\vec{g} + \vec{F}_p^{\,in} + \vec{F}_w + \vec{N} + \vec{F}_\mu \tag{2}$$

where the following forces comprise the Eq. (2):

Gravitational force is expressed with a term $m\vec{g}$, where $\vec{g}$ is the acceleration of the gravity. It is pointed downwards and constant in time.

Inertial transmissive force $\vec{F}_p^{\,in}$ is a fictitious force imposed to the observed body given that it is moving in a non-inertial reference frame. Due to the fact that the reference frame only performs rectilinear motion, this force lacks Coriolis and centrifugal effects and is equal to:

$$\vec{F}_p^{in} = -m\frac{d^2\vec{r}_0}{dt^2} = mA\omega^2\sin\omega t \cdot \vec{e}_0 \tag{3}$$

Air resistance $\vec{F}_w$ is proportional to squared speed of air that flows over the rigid body and air's density, among other factors [8]. Due to the fact that its intensity is relatively low compared to other external forces, it will be neglected in this research.

Surface resistance comprises two orthogonal components: a normal reactive force $\vec{N}$ and a tangential friction force $\vec{F}_\mu$ that arises due to relative contact mechanics between the observed body and the vibratory trough. This research will use the Coulomb's dry friction model with stiction characteristics.

2.1.1 Coulomb's Friction Force

Even though the Coulomb's friction model is among the simplest ones it provides a sufficient approximation for engineering purposes. It is used extensively in contemporary research papers [7, 17, 19, 23] and vibratory conveyor prototypes [3, 4, 13, 22]. In another form of mathematical models that include non-linear functions, exponentials, trigonometry may be more precise, but they carry complex analytical solutions (if there are any) or excessive computer power for their numerical computations, which was shown in [20, 21].

Coulomb's friction force model with the stiction characteristics is defined with two friction coefficients. There is one, static, coefficient during the resting phase μ_s and second, dynamic coefficient when the motion takes place μ_d. Hence there are two significant threshold values of the friction force:

- $F_{\mu,s}$ - the magnitude the opposing exciting force needs to surpass in order for the rigid body to start relative motion. It is equal to $F_{\mu,s}(t) = \mu_s N(t)$
- $F_{\mu,d}$ - the value of the friction force during the relative motion. It changes according to the law $F_{\mu,d}(t) = -\mu_d N(t)\text{sgn}\dot{\xi}$

In the former equation the normal reactive force's intensity is represented as a function of time, even though the body's mass and gravity's acceleration remain constant. Vertical component of the transmissive inertial force $F_{p,\eta}^{in}(t)$ opposes the body's weight $m\vec{g}$ during the backstroke of the actuator and enables the body's relative slippage forward on the vibratory trough.

In the case of vibratory transport, the exciting force is the tangential component of the inertial transmissive force $F_{p,\xi}^{in}$ and the body will start the relative motion when it surpasses the limiting value of the static friction $F_{\mu,s}$.

Right after the motion starts, the friction force rapidly drops from its limiting static value $F_{\mu,s}$ to its dynamic value $F_{\mu,d}$. A graphical representation of this statement is given on the Fig. 2. Horizontal axis shows the intensity and direction of the tangential transmissive force $F_{p,\xi}^{in}$ and the corresponding intensity of the friction force is given on the vertical axis.

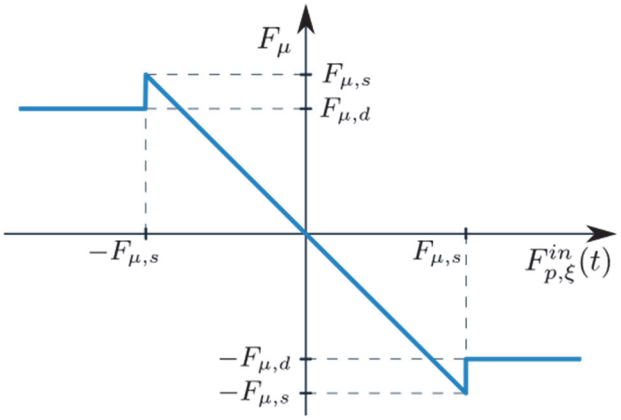

Figure 2 Representation of the Coulomb's friction model with stiction

In a formal mathematical notation, this model of friction can be expressed as a piecewise function as follows:

$$F_\mu(t)=\begin{cases}-F^{in}_{p,\xi}(t) & \text{if } F^{in}_{p,\xi}<|F_{\mu,s}|\\ F_{\mu,s}(t) & \text{if } F^{in}_{p,\xi}=F_{\mu,s}\\ F_{\mu,d}(t) & \text{if } F^{in}_{p,\xi}>|F_{\mu,s}|\end{cases} \tag{4}$$

Therefore, during the state of rest ($\xi = v_r = 0$), the friction force is equal in magnitude to the horizontal component of the translational inertial force, but in the opposite direction $\left(F_\mu=-F^{in}_{p,\xi}(t)\right)$. However, during the relative motion ($\xi = v_r \neq 0$), the friction force is not constant, but varies over time. It takes the value $F_{\mu,d}(t)$, which is time-dependent but does not explicitly depend on the excitation force $F^{in}_{p,\xi}(t)$. At the moment the body begins to move, the magnitude of the friction force ceases to be a function of the excitation force and depends solely on the normal component of the surface reaction force [16].

However, expressing a straightforward dependence of the friction force with respect to relative velocity is a difficult task in the case of Coulomb's friction, given that the force is discontinuous and can take multiple values when the relative velocity is near zero, e.g.:

$$F_\mu(t)=\begin{cases}-F^{in}_{p,\xi}(t) & \text{if } \dot\xi(t)=0\\ F_{\mu,s}(t) & \text{if } \dot\xi(t)=0^+\end{cases} \tag{5}$$

There are several other friction models (e.g., Bengisu-Akay, Stribeck, Benson) that attempt to overcome this issue. For further insight, the reader is invited to consult the literature [16, 21].

Taking into the direction of the motion of the body on the surface, i.e., the values of the sign function, the final expression for the magnitude of the friction force in the case of rigid body motion during the operation of the vibratory conveyor can be roughly formulated as:

$$F_\mu(t)=\begin{cases}\mu_d\cdot N(t) & \text{if } \dot\xi(t)<0\\ -F^{in}_{p,\xi}(t) & \text{if } \dot\xi(t)=0\\ -\mu_d\cdot N(t) & \text{if } \dot\xi(t)>0\end{cases} \tag{6}$$

2.2 Differential Equations of the Relative Motion

By decomposing the Eq. (2) into its vertical and horizontal component, and rearranging the elements the following system of equations is obtained:

$$0=-mg+N(t)+mA\omega^2\omega t\sin\alpha \tag{7}$$

$$m\ddot\xi(t)=F_\mu(t)+mA\omega^2\sin\omega t\cos\alpha \tag{8}$$

From the Eq. (8), the law governing the change of the normal component of the surface reaction force during the operation of the vibratory conveyor can be derived:

$$N(t)=m\left(g-A\omega^2\sin\omega t\right) \tag{9}$$

Since the analysis includes only vibratory regimes without the detachment from the trough, the normal reaction force must remain strictly positive. It reaches a minimum at the sine function's maximum, i.e., when $\sin\omega t = 1$. In this case, the minimum value of the normal force during relative motion is time-invariant and equal to $N_{\min} = m(g - A\omega^2)$, as also derived in [7, 8]. Therefore the minimal reaction force is solely dependent on the type of the vibratory regime, i.e. actuator's amplitude A and angular frequency ω.

Fig. 2 presents vibratory regimes where the rigid body detaches from the surface. Regimes with intermittent contact are marked in red, while those with continuous contact are in green. Since the actuator frequency $f = \omega/2\pi$ is directly controllable via the conveyor driver, it is shown instead of angular frequency ω.

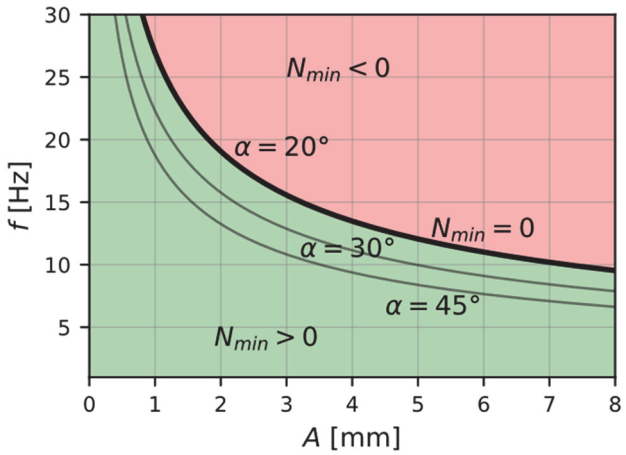

Figure 3 Sign of the normal reaction force for different vibratory regime parameters, shown for various vibration angles and $\mu_s = 0{,}74$

The graph shows curves for various angles of vibration; the curve for $\alpha = 20°$ is plotted as a solid black line, while others are shown as thin lines. As α increases, the curves shift downward, indicating that less intense

vibratory regimes require higher angles to detach the body from the surface.

On the other hand, differential equation given with the Eq. (8) will define the relative velocity $\dot{\xi}(t)$ and relative displacement $\xi(t)$. The sign and the zeros of the function $\dot{\xi}(t)$ determine the intervals of relative rest and motion (slipping) forward or backwards.

The change in the relative coordinate $\xi(t)$ is fundamental to vibratory conveyor operation, as it defines the body's motion relative to the trough and, thus, the flow at the outlet. Determining this function reduces to defining an analytical expression for the friction force F_μ during motion. By substituting the normal reaction force $N(t)$ from Eq. (9) into Eq. (6), we obtain the final piecewise expression for the Coulomb friction force with stiction characteristics:

$$F_\mu(t)=\begin{cases}\mu_d m\left(g-A\omega^2\sin\omega t\sin\alpha\right) & \text{if } \dot{\xi}(t)<0\\ -mA\omega^2\sin\omega t\cos\alpha & \text{if } \dot{\xi}(t)=0\\ -\mu_d m\left(g-A\omega^2\sin\omega t\sin\alpha\right) & \text{if } \dot{\xi}(t)>0\end{cases} \tag{10}$$

Following on, by substituting Eq. (8) into Eq. (6) and after simplifying, the differential equation of motion of the rigid body on the surface during vibratory transport is obtained:

$$\ddot{\xi}(t)=\begin{cases}\mu_d g+A\omega^2\left(\cos\alpha-\mu_d\sin\alpha\right)\sin\omega t & \dot{\xi}<0\\ 0 & \dot{\xi}=0\\ -\mu_d g+A\omega^2\left(\cos\alpha+\mu_d\sin\alpha\right)\sin\omega t & \dot{\xi}>0\end{cases} \tag{11}$$

Also, considering strictly from the perspective of the influence of external forces, previous equation can be also written as:

$$\ddot{\xi}(t)=\begin{cases}0 & F^{in}_{p,\xi}(t)\,£\,|F_{\mu,s}(t)|\\ \left(F^{in}_{p,\xi}(t)+F_{\mu,d}(t)\right)/m & |F^{in}_{p,\xi}(t)|\ >|F_{\mu,s}(t)|\end{cases} \tag{12}$$

Mathematically, the function $\ddot{\xi}(t)$ is discontinuous, with first-order discontinuities at the moments $t=\tau_i$($_i$ = 0, 1, 2, …, n) when relative motion starts or stops. Although the left- and right-hand limits at these points $\left(\ddot{\xi}\left(\tau_i^-\right)\ and\ \ddot{\xi}\left(\tau_i^+\right)\right)$ can be determined, they differ due to the abrupt change in the friction coefficient from static to dynamic at the moment $t=\tau_i$. To obtain the function $\dot{\xi}(t)$, i.e., to integrate $\ddot{\xi}(t)$ over time, it is necessary to define the integration limits for all three subdomains. This requires identifying the exact times when $\dot{\xi}(t)$ changes sign, corresponding to the duration of each motion state.

Fig. 4 illustrates the change of key forces during the relative motion of the body for a representative vibratory regime. Sliding friction coefficients for a steel-steel contact were adopted from the literature [24, 25]. The vibratory trough's horizontal displacement is shown as a black dotted line, magnified 1000 times for clarity. The red thick line represents the tangential inertial force during operation. Positive and negative values of the static friction force are shown by green and blue curves, respectively, with their sign depending on the direction of the inertial force. Effective values are indicated by a solid line and linked with a dashed line for visual clarity. Slipping begins when the inertial force $F^{in}_{p,\xi}$ exceeds the static friction threshold $F_{\mu,s}$, marked by a black square and labelled τ_s on the time axis. After this point, the dynamic friction force (solid pink line) acts on the body until it comes to rest, after which static friction resumes. A dashed pink line indicates the dynamic friction force for potential backward motion, which does not occur in the observed regime.

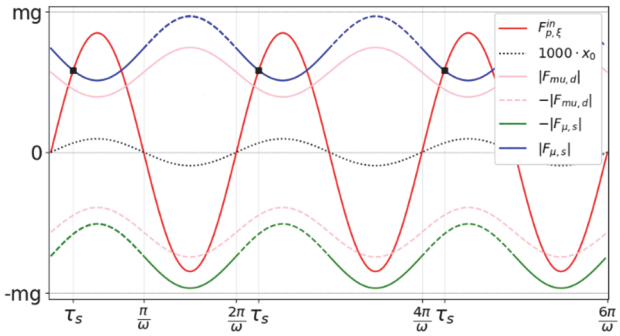

Figure 4 External forces acting on the rigid body during the vibratory process for vibratory parameters f = 15 Hz, A = 1 mm, α = 20°, μ_s = 0,74, μ_d = 0,57

3 THE OCCURRENCE OF THE RELATIVE FORWARD SLIPPING MOTION

Substituting expressions for $F_{\mu,s}$ and $F^{in}_{p,\xi}$ into the condition from Eq. (12) yields the following trigonometric inequality that defines the onset of motion $\left(\ddot{\xi}\neq 0\right)$:

$$\sin\omega t>\frac{\mu_s g}{A\omega^2\left(\cos\alpha+\mu_d\sin\alpha\right)} \tag{13}$$

Since the relative motion is forward, tangential inertial force vector aligns with the positive $O_1\xi$ axis. Given the sine function's periodicity, solutions to Eq. (13) exist only within domains where $\sin\omega t > 0$, i.e., within each odd half-period. Although the sine function is negative in other intervals, no further restrictions are needed because the right-hand side of Eq. (13) remains positive for all relevant physical parameters (i.e. $\forall A, \omega t, \mu_s \in \mathbb{R}^+$, $\forall\alpha\in\left(0,\pi/4\right)$).

To ensure the sine function exceeds the right-hand side expression for some $t\in\mathbb{R}^+$, that expression must be less than or equal to the sine function's maximum value. For given parameters μ_s, μ_d and α this yields the condition the vibratory regime must satisfy to initiate motion of the rigid body:

$$\Phi(A,f)=\frac{\mu_s g}{4\pi^2\cdot Af^2\left(\cos\alpha+\mu_d\sin\alpha\right)}<1 \tag{14}$$

In Fig. 5, the intersection of the surface $\Phi(A, f)$ with the plane $\Phi = 1$ is shown as a solid black curve. The green and red areas indicate regions where $\Phi(A, f) < 1$ and $\Phi(A, f) < 1$, respectively. Thus, the green area marks vibratory regimes that satisfy the condition for forward slippage.

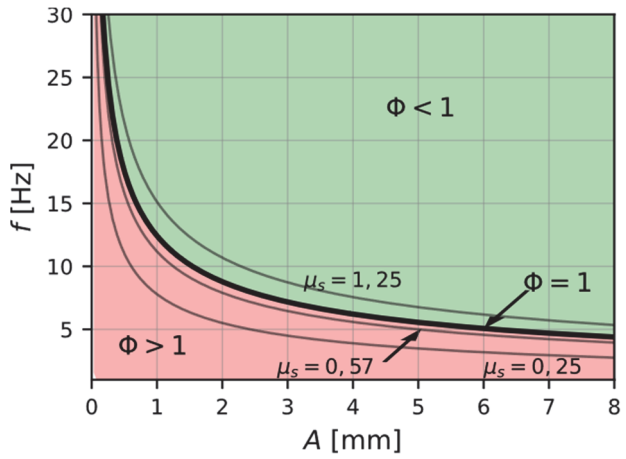

Figure 5 Regions of relative forward slippage for different vibratory regimes, shown for varying values of the static friction coefficient

The representative graph is shown for an angle $\alpha = 20°$. Increasing μ_s (thin curves) shifts the curve $\Phi = 1$ upward. On the other hand, increasing the angle α also shifts the curve upward, but to a lesser extent compared to the influence of the μ_s.

By transforming inequality from Eq. (13) into an equation, one can obtain the exact moments in time when the function $\ddot{\xi}(t)$ takes a value of zero. In other words, it would be the moment right before the body starts a relative motion forward, i.e.:

$$\sin\omega t = \frac{\mu_s g}{4\pi^2 \cdot Af^2\left(\cos\alpha + \mu_d \sin\alpha\right)} \tag{15}$$

If the condition in Eq. (14) holds, the right-hand side of Eq. (15) takes values within (0, 1), since it involves only positive terms and addition. Consequently, the function $y_1 = \sin\omega t$ intersects the straight line $y_2 = \Phi(A, f)$ exactly twice in each odd half-period, as shown in Fig. 6. Additionally, the line $y = 1$ is drawn in black on the graph in Fig. 6, representing the boundary for the forward sliding condition. The x-axis values indicate the moments τ_i when the equality $F^{in}_{p,\xi} = F_{\mu,s}$ holds. Therefore, if $\omega = 2\pi \cdot f$ the solutions to the trigonometric equation in Eq. (15) can be expressed as:

$$\begin{aligned} \tau_{2i} &= \frac{1}{2\pi f}\left(\arcsin\left(\Phi\right) + 2i\pi\right) \\ \tau_{2i+1} &= \frac{1}{2\pi f}\left(\pi - \arcsin\left(\Phi\right) + 2i\pi\right) \end{aligned} \qquad i = 0, 1, 2, ..., n \tag{16}$$

Black squares in Fig. 6 mark the even solutions of Eq. (16), corresponding to potential start times of forward sliding, while red circles mark the odd solutions, which are disregarded.

The body begins to move at the ascending intersections of the curve $y_1 = \sin\omega t$ with the line $y_2 = \Phi(A, f)$. These moments are given by the following relation:

$$\tau_s = \frac{1}{2\pi f}\left(\arcsin\left(\Phi\right) + 2i\pi\right), \quad i = 0, 1, 2, ..., n \tag{17}$$

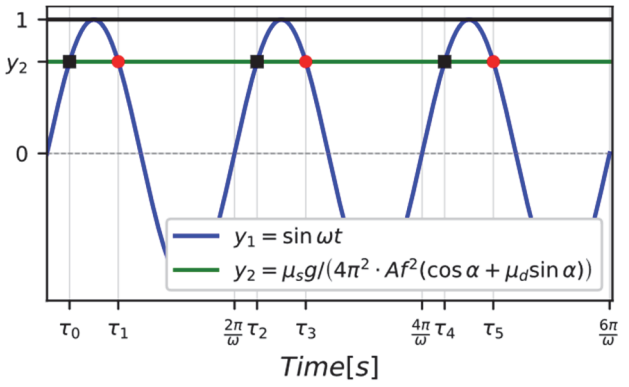

Figure 6 Functions y_1 and y_2 and their intersections

The points τ_{2i+1} from Eq. (16) do not represent the end of forward sliding but merely the second intersection where the equality $F^{in}_{p,\xi} = F_{\mu,s}$ holds. They lack physical meaning, as the static friction condition $F_{\mu,s}$ is not valid during relative motion. The rigid body actually stops sliding in moments τ_t when its relative velocity reaches zero, i.e. $\dot{\xi}(\tau_t)$. A full derivation is provided in the Appendix of this paper and only the final expression is given here.

$$\begin{aligned} \tau_t &= \frac{2\pi Af}{\mu_d g} \cdot Y_\tau + \frac{1}{2\pi f}\left(\arcsin\left(\Phi\right) + 2i\pi\right) \\ Y_\tau &= \left(\cos\alpha + \mu_d \sin\alpha\right)\left(\cos\left(2\pi f \cdot \tau_s\right) - \cos\left(2\pi f \cdot \tau_t\right)\right) \end{aligned} \tag{18}$$

Eq. (18) does not have an analytical solution and must be solved numerically, i.e., with the help of a computer. The characteristic moments used for representative examples in this paper were obtained using the Python software package and its scientific framework SciPy [26]. Only solutions for the first period of motion were calculated, and the remaining moments are simply incremented by the period $T = 2\pi/\omega = f^{-1}$.

Fig. 7 illustrates the dynamics of the rigid bodyb's relative motion on the vibratory conveyor for a representative case. The relative acceleration $\ddot{\xi}(t)$ is shown in purple, with the shaded area under the curve representing its first integral, the relative velocity $\dot{\xi}(t)$. The velocity is plotted in orange and scaled by a factor of 10 for better visibility.

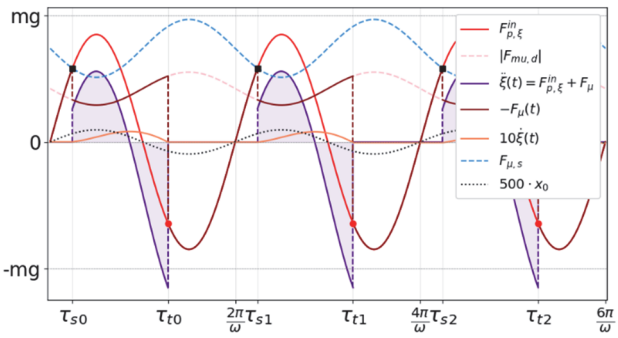

Figure 7: Dynamics of the relative motion during the vibratory process defined f = 15 Hz, A = 1 mm, α = 20°, μ_s = 0,74, μ_d = 0,57 with

As a result of Coulomb's *stiction* and the abrupt change in the friction coefficient from static to dynamic at moments τ_s, the relative acceleration experiences a sudden jump from zero to an initial value $\ddot{\xi}(\tau_s)$. During motion, i.e., within the time interval $t \in [\tau_s, \tau_t] + 2\pi/\omega$, the friction force assumes the current value of the dynamic friction force $F_{\mu,s}(t)$, shown in Fig. 7 as a dashed pink curve. At the moment when the velocity of the rigid body drops back to zero (τ_t), the effective value of the friction force (brown curve) returns to the value of the tangential transmissive inertial force (red curve). The rigid body remains in a state of relative rest until the next moment τ_s when the relative acceleration abruptly increases again, and the body begins to slide forward.

4 COMPUTER EXPERIMENT OF THE RELATIVE MOTION

A typical example of a machine part that must be picked up by an assembly robot in a specified orientation is the self-locking nut. The robot retrieves the nuts from a magazine that needs to be continuously refilled. To simulate the loading process, a 3D model was developed in SolidWorks. The model consists of a vibratory conveyor designed to transport the nut along its trough toward the outlet, as depicted in Fig. 8. Red arrows, shown perpendicular to the direction of the leaf springs, indicate the direction of motion of the trough. The inclination of the leaf springs is exactly α = 20°from the vertical axis.

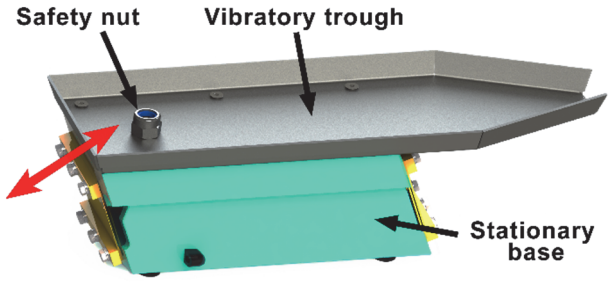

Figure 8 CAD model of the conveyor and initial position of the safety nut on the surface of the vibratory trough

In order to validate the proposed mathematical model, a Motion Analysis package is used. Friction is simulated using the Solid Body Contact feature for friction coefficients μ_s = 0,74 and μ_d = 0,57. The displacement of the trough is defined with a *Linear Motor* feature with an oscillatory form of excitations (f = 15 Hz, A = 1 mm) Gravity is also included using the Gravity feature.

The simulation was performed at 600 frames per second, corresponding to a time increment of 1.667 ms. For the selected excitation frequency of f = 15 Hz, this results in 40 frames per period of the trough's motion. The motion results were extracted in the relative coordinate system. For improved graphical representation, the data were exported to a .csv file, processed in Python, and high-quality plots were generated using the Matplotlib framework.

Fig. 9 shows the intensity of the friction force (blue) and nut's acceleration relative to the trough (red) for first three periods of the vibratory motion. The resemblance to the corresponding values in Fig. 7 is evident, except that in Fig. 9, the acceleration curve is continuous and shows a steep incline at the moments when the nut starts or stops moving. This behaviour can be attributed to the smooth transition from static to dynamic friction.

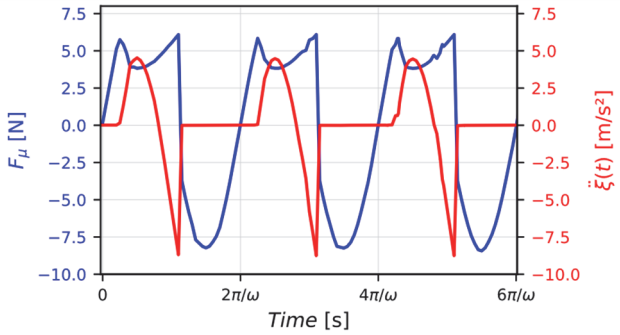

Figure 9 Changes of friction force and relative acceleration over time during the transport of the safety nut

Certain irregularities (noise) appear in the curves during the relative motion phase, i.e., when dynamic friction is active. The jitter observed in these curves in Fig. 9 results from the fact that SolidWorks simulates micro-contacts between the surfaces of the rigid body and the conveyor trough. In other words, the distance between the contacting surfaces is never exactly zero at every time step. It is oscillating around a constant value. This behaviour can be observed if the trajectory of the nut's centre of mass is plotted in its relative coordinate system. Using the Trace Path feature, the data is saved in .csv format, processed in Python and shown in Fig. 10.

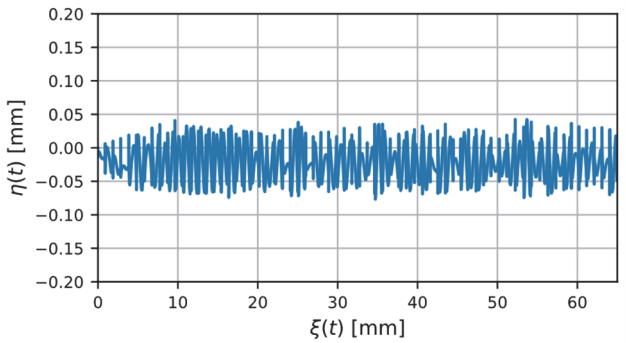

Figure 10 Trajectory of the centre of mass of the nut in non-inertial reference frame during the transport

During the transport, the nut travels more than 60 mm in the horizontal direction. However, its centre of mass oscillates around η = 0 with an amplitude of less than 0,05 mm. As stated before, it is the effect of numerical computations. This oscillation can be approximated as

having a mean value effectively equal to zero, i.e. $\overline{\eta} = \text{const.} \approx 0$.

Changes in the nut's horizontal relative displacement (green curve) and velocity (orange curve) are depicted in Fig. 11. During these slip phases, the nut's relative velocity reaches up to 55 mm/s, with the velocity peaks occurring just when the trough starts its backward motion.

It can be observed that the nut advances by approximately 1 mm with each stroke of the actuator, which results in an exclusive forward-slipping motion that is characterised by resting phases between successive relative slipping occurrences.

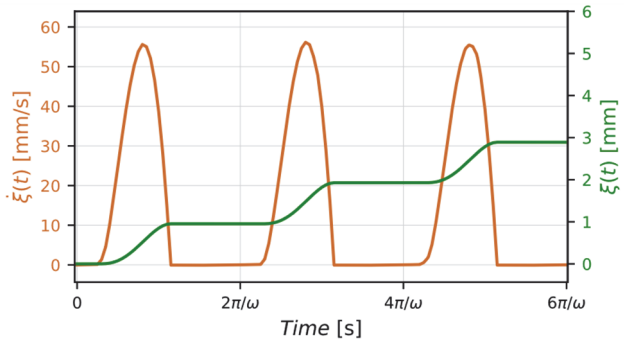

Figure 11 Relative velocity and displacement in non-inertial reference frame during the transport of the nut

Overall, the motion that is depicted in Fig. 11 represents the fundamental principle of vibratory transport with constant contact with the transported object. It consists of multiple smooth relative displacements of the conveyed object. The mathematical model of the vibratory process can therefore be used to estimate the total time required for the nut to traverse the length of the vibratory trough.

5 CONCLUSIONS AND DISCUSSION

This paper covers a practical research about the optimization of the vibratory process for a non-hopping motion of the transported objects. Friction force was modelled with Coulomb's dry friction model with the stiction characteristics.

In the first part of the research, theoretical assumptions were made and differential equations of motions were derived with exact moments in time when the observed body initiates and terminates the relative motion on the vibratory conveyor. Changes in the external forces are shown graphically. Conditions for the vibratory regimes are stated in order to perform the non-hopping motion with the transported object.

Second part of the research covers computer simulation inside SolidWorks Motion Analysis. Extensive simulations were made for small time steps in order to prove the proposed mathematical model.

Overall, this research presents a foundation for future work, where further optimization would be carried on. Some of the potential research directions would be mathematical modelling of the whole vibratory process, observation of unwanted back slip occurrence and real-life experiments on the laboratory equipment with an appropriate control system developed, etc.

Acknowledgement

Results presented in this paper are part of the research supported by the Ministry of Science, Technological Development and Innovation, Republic of Serbia, contracts' number 451-03-136/2025-03/200034 and 451-03-137/2025-03/200105 from 04.02.2025.

6 REFERENCES

[1] Langerholc, M., Zrnić, N., Đorđević, M. et al. (2013). Conveyor design optimization as the provsion of sustainability. *Tehnicki Vjesnik*, *20*(5), 837-846.

[2] Czubak, P. & Lis, A. (2020). Analysis of a New Vibratory Conveyor Allowing for a Sudden Stopping of the Transport. *Tehnicki Vjesnik - Technical Gazette*, *27*(2), 520-526. https://doi.org/10.17559/TV-20181206111514

[3] Buzzoni, M., Battarra, M., Mucchi, E. et al. (2017). Motion analysis of a linear vibratory feeder: Dynamic modeling and experimental verification. *Mechanism and Machine Theory*, *114*, 98-110. https://doi.org/10.1016/j.mechmachtheory.2017.04.006

[4] Despotović, Ž. V., Urukalo, D., Lečić, M. R. et al. (2017). Mathematical modeling of resonant linear vibratory conveyor with electromagnetic excitation: Simulations and experimental results. *Applied Mathematical Modelling*, *41*, 1-24. https://doi.org/10.1016/j.apm.2016.09.010

[5] Ilic, U. & Despotović, Ž. V. (2024). Modeliranje uticaja magnetnog zasićenja na elektromagnetnu silu vibracionog aktuatora. *Proceedings from ENERGETIKA 2024*, 36.

[6] Goncharevich, I. F., Frolov, K. V., & Rivin, E. I. (1990). *Theory of Vibratory Technology (2nd ed.)*. Hemisphere Publishing Coorporation.

[7] Boriskina, Z. M. & Baryshnikova, O. O. (2020). The Mathematical Model of Motion of Particles in Vibrating Conveyors. *International Journal of Mechanical Engineering and Robotics Research*, 76-79. https://doi.org/10.18178/ijmerr.9.1.76-79

[8] Veljić, M., Mladenović, N., & Marković, D. (2010). Optimization of Parameters of a Vibration System for Sorting and Calibrating Deep Frozen Berry Fruits. *Journal on Processing and Energy in Agriculture*.

[9] Najmi, S., Karimi, A. H., Shadmani, M. et al. (2020). A new three-dimensional dynamic model and experimental validation for motion of a part in a vibratory bowl feeder. *Mechanism and Machine Theory*, *143*, 103621. https://doi.org/10.1016/j.mechmachtheory.2019.103621

[10] Balaji, B., Gupta Burela, R., & Ponniah, G. (2022). Dynamics of part motion on a linear vibratory feeder. *Proceedings of the Institution of Mechanical Engineers, Part C: Journal of Mechanical Engineering Science*, *236*(2), 886-893. https://doi.org/10.1177/09544062211012711

[11] Arunyanart, P. & Sudsawat, S. (2023). DEM Simulation for the Predicted Model of Total Rice Seeds Mass in a Vibratory Conveyor. *International Journal of Engineering and Technology*, *15*(4), 161-165. https://doi.org/10.7763/IJET.2023.V15.1240

[12] Vrublevskyi, I. (2024). Vibratory Conveying by Normal Oscillations with Piecewise Constant Acceleration and Longitudinal Harmonic Oscillations. *International Journal for Engineering Modelling*, *37*(1). https://doi.org/10.31534/engmod.2024.1.ri.05v

[13] Vrublevskyi, I. (2023). Increasing of vibratory conveying velocity by optimizing the normal vibration. *Ukrainian Journal of Mechanical Engineering and Materials Science*, *9*(2), 26-35. https://doi.org/10.23939/ujmems2023.02.026

[14] Morcos, W. A. (1970). On the Design of Oscillating Conveyers: Case of Simultaneous Normal and Longitudinal

Oscillations. *Journal of Engineering for Industry*, *92*(1), 53-61. https://doi.org/10.1115/1.3427719
[15] Umbanhowar, P. & Lynch, K. M. (2008). Optimal Vibratory Stick-Slip Transport. *IEEE Transactions on Automation Science and Engineering*, *5*(3), 537-544. https://doi.org/10.1109/TASE.2008.917021
[16] Marques, F., Flores, P., Pimenta Claro, J. C. et al. (2016). A survey and comparison of several friction force models for dynamic analysis of multibody mechanical systems. *Nonlinear Dynamics*, *86*(3), 1407-1443. https://doi.org/10.1007/s11071-016-2999-3
[17] Olsson, H., Åström, K. J., Canudas De Wit, C. et al. (1998). Friction Models and Friction Compensation. *European Journal of Control*, *4*(3), 176-195. https://doi.org/10.1016/S0947-3580(98)70113-X
[18] Haessig, D. A. & Friedland, B. (1990). On the Modeling and Simulation of Friction. *1990 American Control Conference*, 1256-1261. https://doi.org/10.23919/ACC.1990.4790944
[19] Dai, W., Yang, J., & Wiercigroch, M. (2022). Vibration energy flow transmission in systems with Coulomb friction. *International Journal of Mechanical Sciences*, *214*, 106932. https://doi.org/10.1016/j.ijmecsci.2021.106932
[20] Flores, P. (2022). Contact mechanics for dynamical systems: A comprehensive review. *Multibody System Dynamics*, *54*(2), 127-177. https://doi.org/10.1007/s11044-021-09803-y
[21] Pennestrì, E., Rossi, V., Salvini, P. et al. (2016). Review and comparison of dry friction force models. *Nonlinear Dynamics*, *83*(4), 1785-1801. https://doi.org/10.1007/s11071-015-2485-3
[22] Ma, H.-W. & Fang, G. (2016). Kinematics analysis and experimental investigation of an inclined feeder with horizontal vibration. *Proceedings of the Institution of Mechanical Engineers, Part C: Journal of Mechanical Engineering Science*, *230*(17), 3147-3157 https://doi.org/10.1177/0954406215606745
[23] Zughaibi, J. M., Schulze, F. H., & Li, Q. (2018). Critical Velocity of Controllability of Sliding Friction by Normal Oscillations for an Arbitrary Linear Rheology. *Physical Mesomechanics*, *21*(4), 371-378. https://doi.org/10.1134/S1029959918040112
[24] See https://engineeringlibrary.org/reference/coefficient-of-friction
[25] See https://www.engineeringtoolbox.com/amp/friction-coefficients-d_778.html
[26] Virtanen, P., Gommers, R., Oliphant, T. E. et al. (2020). SciPy 1.0: Fundamental algorithms for scientific computing in Python. *Nature Methods*, *17*(3), 261-272. https://doi.org/10.1038/s41592-019-0686-2

Contact information:

Uroš ILIĆ, Research Assistant
(Corresponding author)
University of Belgrade, Institute Mihajlo Pupin,
Volgina 15, 11060 Belgrade, Serbia
E-mail: uros.ilic@pupin.rs

Mihailo LAZAREVIĆ, Full Professor
University of Belgrade, Faculty of Mechanical Engineering,
Kraljice Marije16, 11120 Belgrade, Serbia
E-mail: mlazarevic@mas.bg.ac.rs

Emil VEG, AssociateProfessor
University of Belgrade, Faculty of Mechanical Engineering,
Kraljice Marije16, 11120 Belgrade, Serbia
E-mail: eveg@mas.bg.ac.rs

Željko DESPOTOVIĆ, Principal Research Fellow
University of Belgrade, Institute Mihajlo Pupin,
Volgina 15, 11060 Belgrade, Serbia
E-mail: zeljko.despotovic@pupin.rs

Nenad GUBELJAK, Full Professor
University of Maribor, Faculty of Mechanical Engineering,
Smetanova ul. 17, 20000 Maribor, Slovenia
E-mail: nenad.gubeljak@um.si

A APPENDIX

This appendix covers the integration of relative acceleration during the vibratory motion. As it was mentioned in the main body of this paper, points τ_{2i+1} from Eq. (16) do not define the termination of the relative motion. The body stops when its relative speed comes down to zero, i.e. the moments τ_t for which $\dot{\xi}(\tau_t)=0$. Thus, the body is in relative motion during the open interval $t \in (\tau_s, \tau_t)$, during which it is possible to determine the analytical expression for the velocity function $\dot{\xi}(t)$. Solving the integral of Eq. (12) for the case of relative motion forward $\left(\dot{\xi}(t)>0\right)$ follows:

$$\dot{\xi}(t)=\int\left(-\mu_d g + A\omega^2\left(\cos\alpha+\mu_d\sin\alpha\right)\sin\omega t\right)\mathrm{d}t \tag{19}$$

and by further integration it leads to:

$$\dot{\xi}(t)=-A\omega\left(\cos\alpha+\mu_d\sin\alpha\right)\cos\omega t-\mu_d g\cdot t+C_1 \tag{20}$$

where C_1 is the integration constant, which is obtained from the initial condition when the body starts the relative motion $\left(\dot{\xi}(\tau_s)=0\right)$ and it is equal to:

$$C_1=A\omega\left(\cos\alpha+\mu_d\sin\alpha\right)\cos\omega\tau_s+\mu_d g\cdot\tau_s \tag{21}$$

Following on, if we replace $t=\tau_i$ and $\dot{\xi}(\tau_t)=0$ in Eq. (20) we can find the second moment in the first half-period when the relative velocity is equal to zero, i.e. when the rigid body terminates the relative motion:

$$-A\omega\left(\cos\alpha+\mu_d\sin\alpha\right)\cos\omega\tau_t-\mu_d g\tau_t+C_1=0 \tag{22}$$

After substituting the value of τ_s into the previous equation, we get a transcendental equation for the moments when the rigid body terminates its relative forward slipping on the vibratory conveyor:

$$\begin{aligned}\tau_t&=\frac{2\pi Af}{\mu_d g}\cdot Y_\tau+\frac{1}{2\pi f}\left(\arcsin\left(\Phi\right)+2i\pi\right)\\ Y_\tau&=\left(\cos\alpha+\mu_d\sin\alpha\right)\left(\cos\left(2\pi f\cdot\tau_s\right)-\cos\left(2\pi f\cdot\tau_t\right)\right)\end{aligned} \tag{23}$$

where $\Phi=\mu_s g/\left(4\pi^2\cdot Af^2\left(\cos\alpha+\mu_d\sin\alpha\right)\right)$ and the letter i = 0, 1, 2, …, n represents the number of the half-period covered during the operation of the vibratory conveyor. Additionally, one can easily calculate the length of the interval $\Delta\tau$ during which the rigid body is in relative motion by subtracting the τ_s from τ_t:

$$\Delta\tau=\frac{2\pi Af}{\mu_d g}\cdot Y_\tau \tag{24}$$